

Terrain-dependant Control of Hexapod Robots using Vision

Timon Homberger^{12*}, Marko Bjelonic^{13*},
Navinda Kottege¹, and Paulo V. K. Borges¹

¹ Autonomous Systems Lab, CSIRO, Brisbane, QLD 4069, Australia

² Department of Mechanical and Process Engineering,
ETH Zurich, 8092 Zurich, Switzerland

³ Faculty of Mechanical Engineering,
Technische Universität Darmstadt, 64287 Darmstadt, Germany.

*These authors contributed equally to this work.

Abstract. The ability to traverse uneven terrain is one of the key advantages of legged robots. However, their effectiveness relies on selecting appropriate gait parameters, such as stride height and leg stiffness. The optimal parameters highly depend on the characteristics of the terrain. This work presents a novel stereo vision based terrain sensing method for a hexapod robot with 30 degrees of freedom. The terrain in front of the robot is analyzed by extracting a set of features which enable the system to characterize a large number of terrain types. Gait parameters and leg stiffness for impedance control are adapted based on this terrain characterization. Experiments show that adaptive impedance control leads to efficient locomotion in terms of energy consumption, mission success and body stability.

Keywords: Legged robots; Adaptive control; Stereo vision; Terrain perception; Rough terrain traversal

1 Introduction

Extreme terrain limits the locomotion of mobile robots. Wheeled robots, for example, require an appropriate surface structure for safe maneuvering. Legged robots, on the other hand, are able to adapt their gaits to overcome challenging terrain [1]. One reason why legged robots have gained popularity is because large parts of the Earth's surface are still inaccessible to wheeled machines [2]. Nevertheless, wheeled machines outperform legged robots in many instances due to the complexity of walking machines [3]. It still remains an open challenge to further improve performance of legged machines in the field, especially with a focus on using terrain information to adapt locomotion parameters.

A large number of methods for terrain perception have been discussed in the literature. Such perception is based on exteroceptive sensing [4], proprioceptive sensing [5, 6], or a combination of both [7, 8]. The literature often discriminates between terrain classification and terrain characterization [7], approaching

them as two different problems. Terrain classification aims to associate a surface area with a category in a set of predefined terrain types [9, 10] while terrain characterization tends to assess terrain properties with numeric values, without considering semantics. Aiming for smooth and efficient maneuvering on variable cluttered ground, this work presents a terrain perception system that characterizes the terrain and adapts the virtual stiffness of an impedance controller along with an assessment of the use of step height characterization for stride height adaptation. For this purpose, a highly flexible hexapod robot with 30 degrees-of-freedom (DoF), Weaver [11] is equipped with a vision-based motion adaptation system. The robot and the stereo vision setup are shown in Figure 1. The visual perception module employs a novel method for feature extraction, the “Even run length”, as well as other terrain feature evaluation methods for accurate characterization of a large number of terrain types.

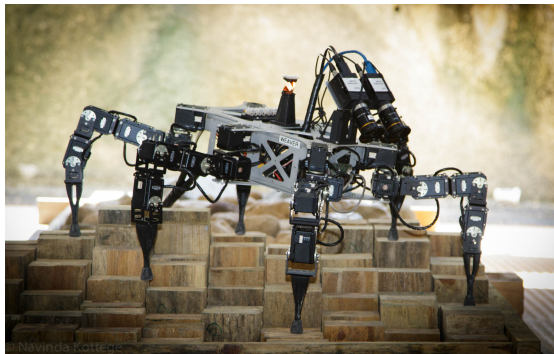


Fig. 1. Hexapod robot Weaver with its stereo camera system on rough terrain.

With its five DoF per leg, Weaver is able to control the orientation and position of the foot tips to maintain ground contact by sensing the force at each foot tip. The legs are controlled analogous to a virtual mass-spring-damper system implemented with a Cartesian space impedance controller. Low virtual stiffness of the legs allows traversing very uneven and cluttered terrain while the robot would get stuck if the legs are very stiff. It was also found that with low virtual stiffness, efficiency decreases for motion on flat terrain. Therefore, the adaptive impedance controller introduced in this paper extends the control strategy described in [11].

2 Terrain-dependant Control

A stereo camera pair is rigidly mounted on the robot such that it captures the terrain immediately in front of the robot. Intrinsic and extrinsic calibration of the stereo pair is realized using the OpenCV stereo calibration package with a checkerboard of known dimensions. The generation of a disparity map (Figure 2) provides depth information of the scene. It is stored as a point cloud in 3D space. This point cloud is downsampled using a voxel grid filter [12] for more



Fig. 2. From left to right: Left camera rectified image, right camera rectified image, disparity map.

efficient spatial transformation. Using an Inertial Measurement Unit (IMU) the data is transformed into a coordinate system which is aligned with the gravity vector. This allows terrain intrinsic feature extraction [12,13]. A Digital Elevation Model (DEM) is generated by discretizing the horizontal plane into quadratic cells [14, 15]. The DEM point cloud consists of the maximum terrain elevation in each cell (Figure 4).

A region of interest (RoI) of the DEM in front of the robot (covering an area equivalent to that of the robot) is defined as the relevant area of interest for terrain characterization, considering that the hexapod is moving forward. A plane is fit into the RoI using a least squares method. From the fitted plane and the DEM data inside the RoI a set of terrain features f_i is extracted. This set is designed to yield distinct characterization of a large number of surface types (Figure 6). The diagram shown in Figure 3 presents the basic pipeline. The features used for ground characterization are detailed in the following:

1) *Center line average* f_1 : Center line average is used to characterize the spread of the elevation data [13].

$$f_1 = \frac{1}{n \cdot m} \cdot \sum_0^n \sum_0^m |z_{data} - z_{plane}| \quad (1)$$

Here, z_{data} denotes the elevation value of a DEM point. z_{plane} is the elevation of the corresponding point of the fitted plane (i.e. $x_{data} = x_{plane}$ and $y_{data} = y_{plane}$). n and m are the dimensions of the considered area, expressed as the number of grid cells of the DEM.

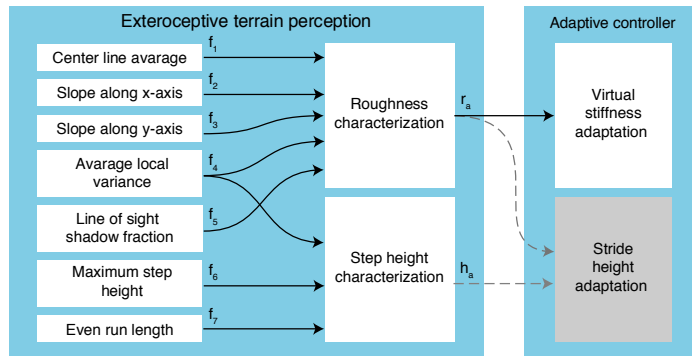


Fig. 3. Overview on exteroceptive terrain perception and adaptive control. The stride height adaptation is part of future work.

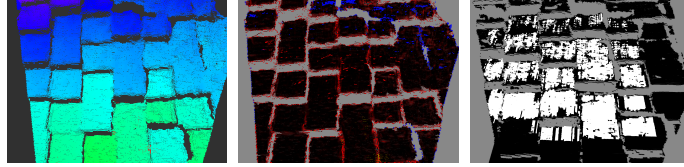


Fig. 4. DEM Point Clouds in three different color schemes, from left to right: Terrain elevation, local variance with red \rightarrow high value, Even run length with white \rightarrow cells within the RoI that appertain to a run.

2) *Slope* f_2 and f_3 : The slope of the fitted plane is the angular difference between the horizontal plane and the plane that was fitted into the elevation data. Different angles in lengthwise and crosswise directions of the robot’s body are the inclination angles of the terrain.

3) *Average local variance* f_4 : Locally distributed variance is derived via a “local descriptor” method. DEM cells in a limited neighborhood to a local descriptor point are considered for variance calculation of the local descriptor cell. Local descriptor method is similarly used in [12, 15]. The spatial average of the local variance (Figure 4) is a measure of the size of ground clutter.

4) *Line of sight shadows* f_5 : There are areas inside the RoI which cannot be perceived by the cameras (Figure 5). These geometrical perception limitations are referred to as “shadows”. These occur if an object/clutter inhibits the cameras lines of sight of reaching certain areas [16]. The system classifies these unperceived areas as uncertainties. The more shadows occur the more conservative the choice of motion parameters, e.g. low leg stiffness.

5) *Maximum step height* f_6 : For sensible adaptation of the stride height, the maximum local change in elevation occurring inside the RoI is determined. A “local descriptor” method is used for calculation. The highest elevation difference detected in a bounded neighbourhood of the local descriptor is the local step height. Maximum step height is the highest step height inside the RoI. A similar approach for maximum step height calculation is used in [15].

6) *Even run length* f_7 : This is a novel method to quantify the amount of continuous, nearly-horizontal surfaces (Figure 4). It is adapted from grey scale image analysis methods [17]. Sequential cells (lengthwise direction) of the DEM are considered to be part of a run if they meet the following two requirements: (1) The elevation of all cells inside a run is within a specified range. (2) The run contains a minimum number of cells. Summing up the total number of cells that are part of a run yields a measure for the tendency of surface patches to be horizontal.

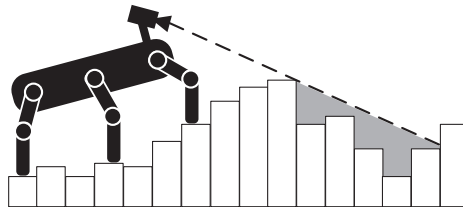


Fig. 5. Shadows caused by line of sight limitations [16].

From subsets of the extracted features f_i , descriptive ground characterization parameters roughness r_a and step height h_a are derived (Figure 3). The roughness and step height are derived by

$$r_a = \frac{1}{a_{norm,1}} \sum_{i=1}^5 a_i \cdot f_i \quad (2)$$

$$h_a = (a_6 \cdot f_6 + a_7 \cdot f_4 \cdot f_7) / (a_{norm,2}) \quad (3)$$

The weighting parameters a_i are set empirically, i.e. by defining suitable r_a and h_a for a number of exemplary surface types. The parameters r_a and h_a are dimensionless values between zero and one. These parameters are used for adaptive impedance control and future stride height adaptation respectively (Figure 3).

The formula for step height characterization (3) includes the term: $a_7 \cdot f_4 \cdot f_7$. This correction term quantifies the occurrence of nearly planar surfaces which are bordered by slopes. It was found that this kind of terrain requires high stride height to be smoothly traversed. This novel method is designed to enable the robot to traverse terrain with sharp drop-offs/inclines (e.g. curbs, steps) by adding an extra margin to the maximum step height f_6 . The system uses terrain characterization rather than classification to achieve this task [7]. Characterization results are presented in Section 4.

Adaptive impedance control sets the virtual stiffness c_{virt} depending on the vision based roughness estimation r_a . A suitable correlation between virtual stiffness and roughness gives a third order polynomial:

$$c_{virt} = b_0 + b_1 \cdot r_a + b_2 \cdot r_a^2 + b_3 \cdot r_a^3 \quad (4)$$

It is derived by choosing desired (optimal) stiffness values for a variety of terrain types. A set of roughness/stiffness data points are chosen along with the corresponding roughness estimates and a curve is fit over these points using minimizing least squares error yielding (4).

As the robot perceives the roughness r_a and step height h_a characterization at a given distance in front of the platform, information on ego-motion is needed. An external position estimation system described in Section 3 is used to provide the robot with its relative position, which is used to derive the required ego-motion information. The visually perceived terrain characterization is associated with a point in horizontal 2D space. This point lies centrally inside the RoI of the DEM. In each time frame the area which contains the robot's vertical projection to the ground is searched for the point with the highest corresponding roughness and step height value. This ensures sufficiently low stiffness (and sufficiently high stride height respectively) to overcome rough terrain.

3 Experiments

For comparative evaluation of performance, a multi-terrain testbed of 8.4 m length was used for experimentation. It consists of patches of six different terrain types (Figure 6). Terrain types include flat ground (A), planar slope (B),

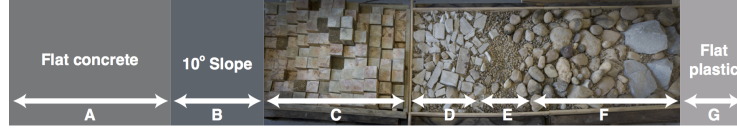


Fig. 6. Multi-terrain testbed: 2.93 m of flat ground (segment A) followed by 1.2 m of inclined planar segment (10°) (segment B) are traversed before entering segment C. Maximum height difference: 113 % (segment C), 28 % (segment D), 11 % (segment E) and 72 % (segment F) of Weavers body height.

wooden cuboid blocks (C) and cluttered terrain consisting of crumbled concrete, sand, pebbles and variably sized stones (D-F). The experiments consisted of the hexapod robot repeatedly traversing this testbed with high level navigation (velocity commands) provided by a human operator via joystick. A sample video of the operation is available online⁴.

For evaluation of the motion efficiency, the cost of transport CoT is defined as

$$CoT = P/(mgv) \quad (5)$$

where P is the power consumption, m is the mass of the robot, g is the gravitational acceleration and v is the velocity of the robot. The power consumption $P = UI$ was measured at 20 Hz by an Arduino based sensor system. This sensor monitors the voltage U and current I of the power supply. Weaver’s mass is 9.3 kg. A robotic total station (Leica TS12) was used during testing to track the position of the robot at 4 Hz. The total station tracks a reflector prism attached to the robot and provides its 3D position. This ego-motion measurement serves as input to the terrain characterization as described in the end of Section 2. In addition, the velocity of the robot in (5) is approximated by finite differences of the position for evaluation of the robot’s cost of transport (CoT).

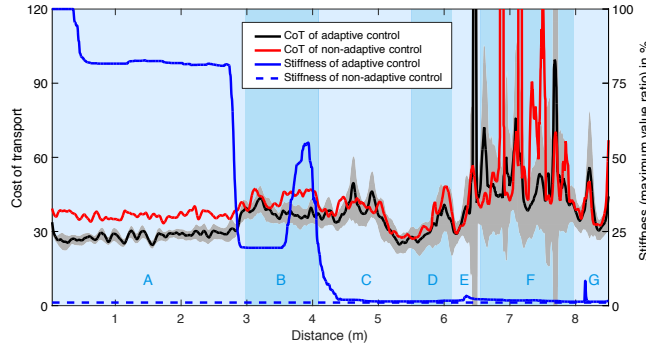


Fig. 7. The CoT of the adaptive (black line) and non-adaptive controller (red line) shows the mean of eight runs on the testbed. One standard deviation of the adaptive controller is shaded in grey. In addition, the virtual stiffness of the adaptive and non-adaptive controller is shown.

⁴Video available here: <https://confluence.csiro.au/display/ASL/ISER2016Stereo>

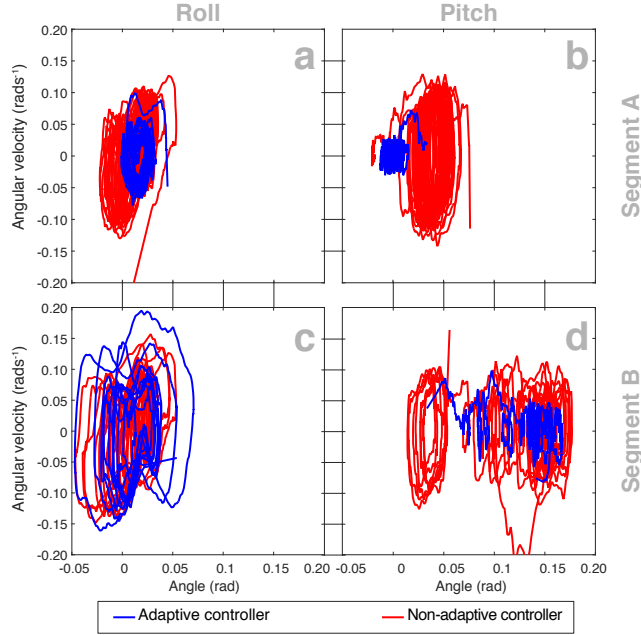


Fig. 8. Limit cycles of the roll and pitch movement projected onto the phase plane for segments A and B of the multi-terrain testbed (based on IMU data).

Two sets of eight runs each have been conducted to examine the CoT. Adaptive impedance control was used during the first set and constant stiffness was applied in the second set. The range of the virtual stiffness of the adaptive controller is set between 1060 Nm^{-1} and 70340 Nm^{-1} . The constant stiffness of the non-adaptive impedance controller is the minimum of the range of stiffness values of the adaptive impedance control (i.e. 1060 Nm^{-1}). Thus, it allows to overcome the most difficult segments of the multi-terrain testbed.

4 Results and Analysis

Adaptive Impedance Control The resulting CoT of the experiments described in Section 3 are displayed in Figure 7. The difference in CoT in segments A and B can be explained by angular and vertical robot body motion which occurs if walking on flat ground or planar slope with a low stiffness. The CoT reduction of adaptive impedance control is especially high in segment B since the body motion (non-adaptive case) causes instability and slippage on the slope. The additional body motion of the non-adaptive controller is shown in Figure 8. It can be seen that the limit cycles of roll and pitch movement is reduced by the adaptive controller in segment A and B. During transition from flat ground to planar slope CoT is increased in both sets. On rough terrain (segments C to F) the two sets have similar CoT. This matches expectations as there is no significant difference of virtual stiffness. The adaptive controller reduces the CoT

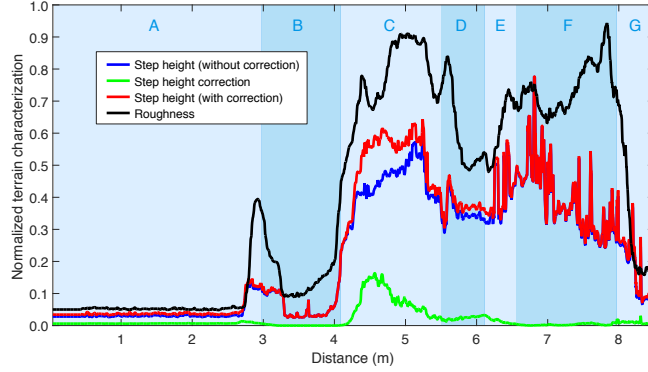


Fig. 9. Mean of step height characterisation terms and roughness characterization with the eight runs using adaptive impedance control.

by 23% (segment A), 13% (segment B), 3% (segment C), 10% (segment D), 2% (segment E) and 29% (segment F). This also shows the value of adapting the virtual stiffness by a small amount on rough terrain. Especially in segment F the adaptive controller reduces high CoT spikes which occurs when the robot approaches zero velocity.

Step Height Characterization The step height characterization term h_a in (3) serves as input for terrain dependant stride height adaptation⁵. As can be seen in Figure 9 the correction term adds an extra margin to the corrected stride height h_a during traversal of segment C of the testbed. This segment consists of wooden cuboid blocks and therefore contains horizontal surface patches with vertical transitions. Therefore the system detects long run lengths and high average local variance simultaneously. In all the other segments the correction

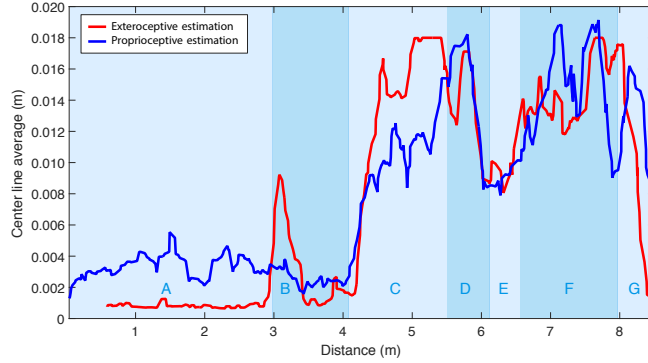


Fig. 10. Comparison of center line average estimation: proprioceptive (foot tip positions) and exteroceptive (vision based terrain perception).

⁵ Adaptive stride height will be addressed in future work.

term is close to zero as either average local variance f_4 or the even run length f_7 is close to zero (no continuous horizontal surfaces).

In segment B (planar slope) a higher stride height is desired to be set than during traversal in segment A (flat ground). Corrected step height does not provide discrimination between segments A and B as can be seen in Figure 9. To achieve this discrimination h_a can be considered to be complemented by the roughness r_a .

Centerline Average Estimation In Figure 10 shows verification results of the visual extraction of center line average. It is measured along the testbed and compared to the proprioceptive estimation of the center line average. The latter is derived from the foot tip positions using forward kinematics [11]. It can be seen that both estimations of the center line average coincide with each other on uneven terrain (segments C to F). There is a constant offset between the two estimations on flat terrain (segment A) and the proprioceptive estimation does not recognize the transition from flat (segment A) to inclined terrain (segment B) because the stiffness is too high to adapt the foot tip positions.

5 Conclusions

This work presented a stereo vision based terrain sensing method for a hexapod robot. The system characterizes the terrain in front of the robot and adapts the virtual stiffness of the impedance controller as well as the stride height. The experimental results with the hexapod platform Weaver showed significant efficiency improvements. In particular, the robot managed to efficiently traverse the multi-terrain testbed. Adaptive impedance control showed slightly better performance on very uneven terrain while it significantly lowered CoT for motion on flat and inclined terrain. In addition, body stability was improved by adaptive impedance control as well. The robot chose optimal virtual stiffness values depending on the traversed terrain. Moreover, the feature perception system demonstrated the ability of the presented terrain analysis method to characterize nearly even surface patches which are bordered by steep slopes. Adapting the robot's stride height accordingly benefits application scenario in which the robot is confronted with man-made structures such as curbs or steps.

References

1. Bares, J.E., Whittaker, W.L.: Configuration of autonomous walkers for extreme terrain. *The International Journal of Robotics Research* **12**(6) (1993) 535–559
2. Belter, D., Walas, K.: A compact walking robot - flexible research and development platform. In Szewczyk, R., Zieliński, C., Kaliczyńska, M., eds.: *Recent Advances in Automation, Robotics and Measuring Techniques*. Volume 267 of *Advances in Intelligent Systems and Computing*. Springer (2014) 343–352

3. Görner, M., Wimböck, T., Baumann, A., Fuchs, M., Bahls, T., Grebenstein, M., Borst, C., Butterfass, J., Hirzinger, G.: The DLR-Crawler: A testbed for actively compliant hexapod walking based on the fingers of DLR-Hand II. In: IEEE/RSJ International Conference on Intelligent Robots and Systems (IROS). (2008) 1525–1531
4. Bellutta, P., Manduchi, R., Matthies, L., Owens, K., Rankin, A.: Terrain perception for DEMO III. In: IEEE Intelligent Vehicles Symposium. (2000) 326–331
5. Coyle, E., Jr., E.G.C., Roberts, R.G.: Speed independent terrain classification using singular value decomposition interpolation. In: IEEE International Conference on Robotics and Automation (ICRA). (2011) 4014–4019
6. Tsujita, K., Matsuda, M., Masuda, T.: An adaptive locomotion of a quadruped robot on irregular terrain using simple biomimetic oscillator and reflex controllers without visual information. In: IEEE International Conference on Robotics and Biomimetics (ROBIO). (Dec 2010) 1358–1363
7. Krebs, A., Pradalier, C., Siegwart, R.: Comparison of Boosting Based Terrain Classification Using Proprioceptive and Exteroceptive Data. In: Experimental Robotics. Springer Berlin Heidelberg (2009) 93–102
8. Brooks, C.A., Iagnemma, K.: Vibration-based terrain classification for planetary exploration rovers. IEEE Transactions on Robotics **21**(6) (2005) 1185–1191
9. Best, G., Moghadam, P., Kottege, N., Kleeman, L.: Terrain classification using a hexapod robot. In: Australasian Conference on Robotics and Automation (ACRA). (2013)
10. Christie, J., Kottege, N.: Acoustics based terrain classification for legged robots. In: IEEE International Conference on Robotics and Automation (ICRA). (2016)
11. Bjelonic, M., Kottege, N., Beckerle, P.: Proprioceptive control of an over-actuated hexapod robot in unstructured terrain. In: To appear in IEEE/RSJ International Conference on Intelligent Robots and Systems (IROS). (2016)
12. Bellone, M., Reina, G., Giannoccaro, N.I., Spedicato, L.: Unevenness point descriptor for terrain analysis in mobile robot applications. International Journal of Advanced Robotic Systems **10** (2013)
13. Hoffman, R., Krotkov, E.: Terrain roughness measurement from elevation maps. In: Advances in Intelligent Robotics Systems Conference. (1990) 104–114
14. Aeschmann, R., Borges, P.V.K.: Ground or obstacles? detecting clear paths in vehicle navigation. In: IEEE International Conference on Robotics and Automation (ICRA). (2015) 3927–3934
15. Chilian, A., Hirschmüller, H.: Stereo camera based navigation of mobile robots on rough terrain. In: IEEE/RSJ International Conference on Intelligent Robots and Systems (IROS). (2009) 4571–4576
16. Kolter, J.Z., Kim, Y., Ng, A.Y.: Stereo vision and terrain modeling for quadruped robots. In: IEEE International Conference on Robotics and Automation (ICRA). (2009) 1557–1564
17. Theodoridis, S., Koutroumbas, K.: Pattern Recognition, Third Edition. Academic Press, Inc., Orlando, FL, USA (2006)